

# Constraining the $\alpha$ -nucleus potential for $\alpha$ -decay calculation with nuclear rainbow scattering

Nguyen Tri Toan Phuc<sup>1,2</sup>, Le Hoang Chien<sup>1,2,\*</sup>, Chau Van Tao<sup>1,2</sup>



Use your smartphone to scan this QR code and download this article

<sup>1</sup>Department of Nuclear Physics, Faculty of Physics and Engineering Physics, University of Science, 227 Nguyen Van Cu, District 5, Ho Chi Minh City, Vietnam

<sup>2</sup>Vietnam National University, Ho Chi Minh City, Vietnam

## Correspondence

**Le Hoang Chien**, Department of Nuclear Physics, Faculty of Physics and Engineering Physics, University of Science, 227 Nguyen Van Cu, District 5, Ho Chi Minh City, Vietnam

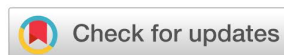
Vietnam National University, Ho Chi Minh City, Vietnam

Email: lhchien@hcmus.edu.vn

## History

- Received: 2021-11-07
- Accepted: 2022-03-16
- Published: 2022-03-31

DOI : 10.32508/stdj.v25i1.3857



## Copyright

© VNUHCM Press. This is an open-access article distributed under the terms of the Creative Commons Attribution 4.0 International license.



## ABSTRACT

**Introduction:** The emission of  $\alpha$  particles is a powerful probe for the  $\alpha$ -cluster structure of heavy nuclei. The  $\alpha$ -nucleus potential is a crucial ingredient in the  $\alpha$ -decay calculation within the preformed cluster model. One of the most reliable ways to construct this potential is the double-folding model, where an effective nucleon-nucleon interaction is folded with the nuclear densities. In the folding model calculation, there are many ambiguities in the choice of the nuclear densities of the daughter nucleus for  $\alpha$ -decay. We propose to directly constrain the  $\alpha$ -nucleus potential for  $\alpha$ -decay and choose the daughter nuclear density using the nuclear rainbow scattering phenomenon. **Methods:** The refractive rainbow pattern in the elastic scattering cross section within the optical model can probe deep into the interior region of the  $\alpha$ -nucleus potential. We apply this method to investigate the reliability of the nuclear potential used in the  $\alpha$ -decay of the  $^{212}\text{Po}$  nucleus leading to the  $^{208}\text{Pb}$  daughter nucleus by examining the elastic  $\alpha$  scattering on  $^{208}\text{Pb}$ . In such an approach, we perform the double-folding calculation to construct the  $\alpha$ -nucleus potential using several common parametrizations of the daughter nuclear densities. These parametrizations include the mean-field Hartree-Fock-Bogoliubov calculations with the BSk14 and D1S interactions, the independent particle model, and the 2-parameter Fermi distributions. The obtained nuclear potentials are applied to the optical model to calculate the elastic  $\alpha$ - $^{208}\text{Pb}$  scattering cross sections that are compared with the experimental data. These nuclear potentials are further used in the preformed cluster model to study the  $\alpha$ -decay half-life of  $^{212}\text{Po}$ . **Results:** The nuclear densities from the Hartree-Fock-Bogoliubov calculations are shown to provide the best description for both the nuclear rainbow scattering and  $\alpha$ -decay half-life. The results indicate a strong correspondence between the capabilities of the nuclear potential to reproduce the cross section of  $\alpha$  scattering and the  $\alpha$ -decay half-life. The extracted  $\alpha$  preformation factors from the semiclassical preformed cluster model with folding potentials are in good agreement with those from other studies. **Conclusion:** The nuclear rainbow scattering phenomenon can be used to provide reliable  $\alpha$ -nucleus potential for  $\alpha$ -decay studies within the preformed cluster model. The nuclear densities from the mean-field Hartree-Fock-Bogoliubov method with the BSk14 and D1S interactions are the appropriate choices for the DFM calculation used in the  $\alpha$ -decay study.

**Key words:**  $\alpha$ -decay, double-folding model, nuclear density, nuclear rainbow scattering

## INTRODUCTION

The  $\alpha$ -decay process is a valuable tool to probe the structure of the atomic nucleus<sup>1-3</sup>. One of the most commonly used models to describe the  $\alpha$ -decay half-lives is the preformed cluster model<sup>4</sup>, which assumes that the  $\alpha$  particle is formed inside the nucleus and emits through the Coulomb barrier by the quantum tunneling effect. The probability for the  $\alpha$  cluster to be formed before emission is called the  $\alpha$  preformation factor and is directly related to the  $\alpha$  cluster structure of the nucleus. By comparing the calculated  $\alpha$ -decay half-lives with those from experimental data, many important aspects of the  $\alpha$  clustering for heavy nuclei ( $A > 100$ ) can be examined. With advances in experimental capability, we can now measure the  $\alpha$ -decay of many exotic nuclei<sup>2,3,5</sup>. Finally, the  $\alpha$ -decay plays

a critical role in the identification of new chemical elements in the synthesis of superheavy elements<sup>6,7</sup>.

In the preformed cluster model, the  $\alpha$ -decay half-life can be determined from the  $\alpha$  preformation factor, assault frequency, and transmission probability. The assault frequency is the number of collisions per second between the  $\alpha$  particle and the Coulomb barrier, while the transmission probability governs the likelihood that the  $\alpha$  particle tunnels through the barrier. In the semiclassical framework of the preformed cluster model<sup>4</sup>, both the assault frequency and transmission probability can be uniquely determined with an  $\alpha$ -nucleus potential between the emitted  $\alpha$  particle and the daughter nucleus. It has been shown that the double-folding model (DFM)<sup>8,9</sup> can provide a consistent framework to reliably calculate the  $\alpha$ -nucleus po-

**Cite this article :** Phuc N T T, Chien L H, Tao C V. Constraining the  $\alpha$ -nucleus potential for  $\alpha$ -decay calculation with nuclear rainbow scattering. *Sci. Tech. Dev. J.*; 25(1):2288-2296.

tential<sup>10-14</sup>. By folding the effective nucleon-nucleon (NN) interaction with the nuclear densities of the  $\alpha$  particle and daughter nucleus, the DFM significantly reduces the number of free parameters and provides a firm microscopic basis for the  $\alpha$ -decay calculation. Although the DFM offers a much better consistency compared to other phenomenological descriptions of the  $\alpha$ -nucleus potential, it is not completely free from ambiguity. One of the largest ambiguities in the folding model that has a direct impact on the  $\alpha$ -decay half-life is the choice of the daughter nuclear density. Since most realistic effective NN interactions are also density dependent, the input densities play a major role in the DFM calculation<sup>8,9</sup>. In contrast to the density of the  $\alpha$  particle, which can be accurately described with a Gaussian form<sup>9,15</sup>, the exact density of the daughter nucleus is not well-known, especially for nuclei far from the valley of stability. This is the case for most systematic analyses of  $\alpha$ -decay half-lives, where the number of considered nuclei is large and most of them do not have an experimentally determined density. Therefore, the densities calculated from microscopic structure models or global parametrizations are usually adopted. Regardless of its importance, the impact of the daughter nuclear density used in the DFM on the calculated half-life is rarely systematically checked. Moreover, there are very few studies, such as Refs.<sup>11,16</sup> that can ensure the same DFM with a specific choice density used in the  $\alpha$ -decay calculation can also be consistently used for other  $\alpha$ -related processes, such as fusion, scattering, and transfer reactions.

It is well-known that the nuclear rainbow phenomenon exhibited in nucleus-nucleus scattering can probe the nucleus-nucleus potential down to a very small internuclear distance with high sensitivity<sup>8,17</sup>. The rainbow effect is characterized by the notable refractive Airy pattern in the scattering cross section. This distinguished pattern is caused by the interference of the traveling waves that probe deep inside the nucleus and survive its absorption. The capability to constrain the optical potential with the nuclear rainbow effect is first observed in the scattering of  $\alpha$  on heavy nuclei<sup>18-20</sup>. They are also among the systems that display the strongest refractive patterns. Only a realistic description of  $\alpha$ -nucleus potential can faithfully reproduce the Airy minima in the  $\alpha$ -nucleus scattering cross section. Several studies have suggested that the  $\alpha$ -nucleus folding potential capable of reproducing the rainbow effect can also accurately describe the  $\alpha$ -cluster structure of the composite nucleus<sup>10,21</sup>. These findings imply that the folding

potential required in the  $\alpha$ -decay calculation can be constrained by refractive  $\alpha$ -nucleus scattering.

In this work, we propose to use the nuclear rainbow effect observed in elastic  $\alpha$ -nucleus scattering to constrain the nuclear potential and evaluate several choices of daughter nuclear densities used in the double-folding calculation of the  $\alpha$ -decay half-life. We benchmark our approach for the  $\alpha$ -decay of <sup>212</sup>Po leading to the <sup>208</sup>Pb core, which is an extensively studied process due to the double-magic nature of the daughter nucleus<sup>22-24</sup>. In this method, the elastic  $\alpha + ^{208}\text{Pb}$  scattering cross section calculated by the DFM with different densities is compared with the experimental data at 139 MeV<sup>19</sup>, where a clear nuclear rainbow pattern can be observed. We also demonstrate the sensitivity of the nuclear rainbow effect to the range parameter used in the Coulomb potential prescription.

## COMPUTATIONAL METHODS

### Double-folding model

Here, we briefly introduce the formalism of the DFM used to calculate the  $\alpha$ -nucleus potential between the  $\alpha$  particle and the daughter nucleus. A more detailed description can be found in Ref.<sup>9</sup>. In the DFM, the antisymmetrized nucleus-nucleus potential can be written as a Hartree-Fock-type potential

$$V_N = V_D + V_{EX} = \sum_{i \in \alpha, j \in A} [\langle ij | v_D | ij \rangle + \langle ij | v_{EX} | ji \rangle], \quad (1)$$

where A denotes the daughter nucleus or the core of the composite  $\alpha$ -emitted nucleus and  $|i\rangle, |j\rangle$  are the single-particle wave functions of the  $\alpha$  particle and daughter nucleus, respectively.  $v_D$  and  $v_{EX}$  are the direct and exchange parts of the effective NN interaction, respectively. In the DFM, the  $V_{EX}$  account for a single-nucleon knock-on exchange of two nucleons, each belonging to a participating nucleus.

Following the prescription of Eq. (1), the local direct part of the double-folding potential at the distance R can be written in terms of one-body densities as

$$V_D(E, R) = \int \rho_\alpha(r_\alpha) \rho_A(r_A) v_D(\rho, E, s) d^3 r_\alpha d^3 r_A, \\ s = r_A - r_\alpha + R,$$

where E is the center-of-mass energy and  $\rho_\alpha$  and  $\rho_A$  are the nuclear densities of the  $\alpha$  particle and daughter nucleus, respectively. The descriptions for these densities will be extensively discussed in a later part of this paper.

We use the local approximated form for the exchange part

$$V_{EX}(E, R) = \int \rho_{\alpha}(r_{\alpha}, r_{\alpha}) v_{EX}(\rho, E, s) \times \exp\left(\frac{iK(E, R)s}{M}\right) d^3r_{\alpha} d^3r_A$$

The recoil factor  $M=4A/(4+A)$  with  $A$  is the mass number of the daughter nucleus. The density matrix approximation<sup>25</sup> is applied for the densities in (3). The self-consistent relative momentum is given by

$$K^2(E, R) = \frac{2\mu}{\hbar^2} [E - V_D(E, R) - V_{EX}(E, R) - V_C(R)], \quad (4)$$

where  $V_C(R)$  is the Coulomb potential and  $\mu$  is the reduced mass. The Coulomb potential in the main results of this work is obtained by folding two uniform charge spheres<sup>26</sup> with the  $R_C$  values of  $\alpha$  and  $^{208}\text{Pb}$  nuclei chosen to reproduce the experimental root-mean-square (RMS) charge radii<sup>27</sup> through the formula  $R_C = \sqrt{(5/3)r_{RMS}^2}$ <sup>28</sup>.

In this work, we use the density-dependent CDM3Y3 parametrization<sup>29</sup> for the effective NN interaction in Eqs. (1)-(3)

$$v_{D(EX)}(\rho, E, s) = (1 - 0.003 \epsilon) F(\rho) v_{D(EX)}(s), \quad (5)$$

where  $\epsilon$  is the incident energy per nucleon and  $v_{D(EX)}(s)$  is the direct (exchange) term of the density-independent M3Y-Paris interaction<sup>30</sup>. The density-dependent term is parametrized as

$$F(\rho) = C \left[ 1 + \alpha e^{-\beta\rho} - \gamma\rho \right], \quad (6)$$

with  $C=0.2985$ ,  $\alpha=3.4528$ ,  $\beta=2.6388$  ( $\text{fm}^3$ ), and  $\gamma=1.5$  ( $\text{fm}^3$ ) chosen to reproduce the saturation properties of the symmetric nuclear matter. The overlapping density  $\rho$  follows the so-called frozen density approximation<sup>29</sup>.

We note that although the DFM has been adopted in many  $\alpha$ -decay calculations<sup>10-14</sup>, the use of a realistic density-dependent NN interaction with the finite-range exchange term for this type of calculation is still very limited<sup>31</sup>. Many studies have shown that the finite-range exchange term and the density dependence of the NN interaction in the DFM are strongly required to describe the rainbow feature in the elastic scattering cross section (see Refs.<sup>8,9,17</sup> and references therein).

### $\alpha$ -decay calculation

In this work, the  $\alpha$ -decay half-life is calculated using the preformed cluster model with the Wentzel-Kramers-Brillouin (WKB) approximation<sup>4</sup> as

$$T_{1/2} = \frac{\hbar \ln 2}{\Gamma} \quad (7)$$

where the  $\alpha$ -decay width is determined as

$$\Gamma = \frac{\hbar P_{\alpha} v}{1 + \exp(x)}, \quad (8)$$

$$x = 2 \int_{R_2}^{R_3} \sqrt{\frac{2\mu}{\hbar^2} (V_T(R) - Q_{\alpha})} dR,$$

where  $P_{\alpha}$  is the  $\alpha$  preformation factor,  $Q_{\alpha}$  is the  $\alpha$ -decay Q-value, and  $\mu$  is the reduced mass of the  $\alpha$ -core system. The assault frequency in the semiclassical system is given by

$$v = \frac{\hbar}{2\mu} \left[ \int_{R_1}^{R_2} \left[ \frac{2\mu(Q_{\alpha} - V_T(R))}{\hbar^2} \right]^{-\frac{1}{2}} dR \right]^{-1}. \quad (9)$$

The classical turning points  $R_1, R_2, R_3$  are obtained from the condition

$$V_T(R_1) = V_T(R_2) = V_T(R_3) = Q_{\alpha}. \quad (10)$$

The total potential  $V_T$  in the WKB approximation is given by

$$V_T(R) = \lambda V_N(R) + V_C(R) + V_L(R), \quad (11)$$

where  $V_N(R)$  is the double-folding potential in Eq. (1),  $V_L(R)$  is the centrifugal potential in the Langer form<sup>4</sup> characterized by the orbital angular momentum  $L$ . The normalization factor is uniquely determined by the Bohr-Sommerfeld quantization condition<sup>4</sup>

$$\int_{R_1}^{R_2} \sqrt{\frac{2\mu}{\hbar^2} (Q_{\alpha} - \lambda V_N(R) - V_C(R) - V_L(R))} dR = (G - L + 1) \frac{\pi}{2},$$

where the orbit global quantum number  $G=22$  follows the Wildermuth-Tang rule<sup>4,32</sup>.

## RESULTS

### Impacts of nuclear density on the folding potential

First, we examine several descriptions of the nuclear densities, especially those for the daughter nucleus, and investigate their impacts on the double-folding potential. For the  $\alpha$  particle density, we use the Gaussian shape  $\rho_{\alpha}(r) = 0.4229 \exp(-0.7024r^2)$  from Ref.<sup>15</sup>, which is universally adopted in almost all  $\alpha$ -decay and scattering calculations.

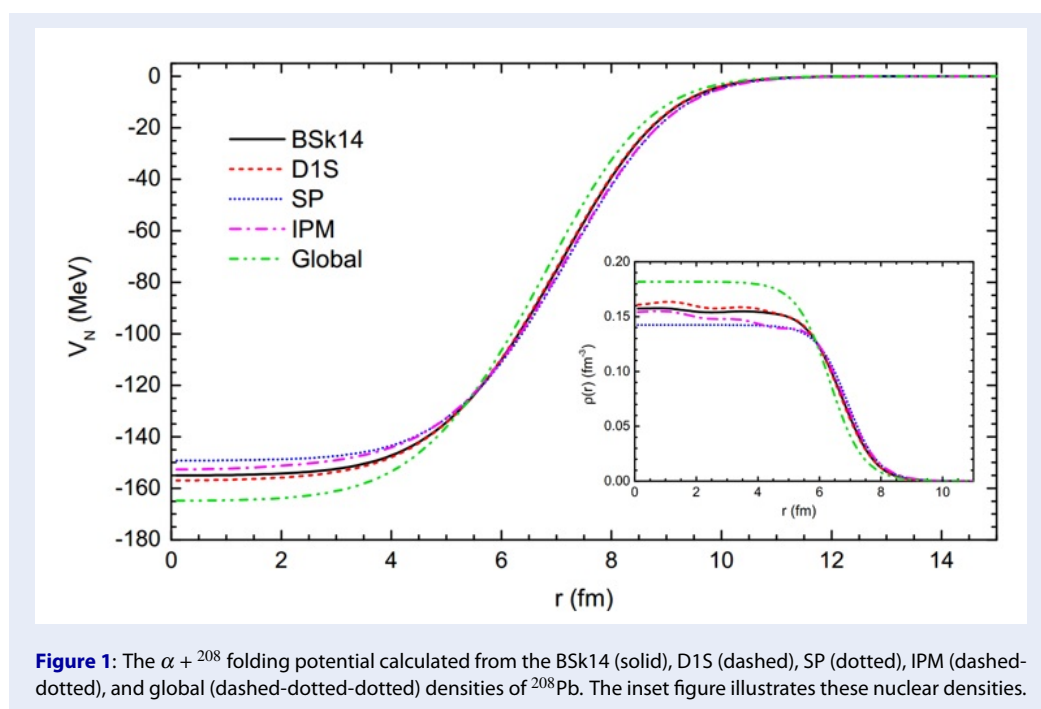


**Figure 1:** The  $\alpha + {}^{208}\text{Pb}$  folding potential calculated from the BSk14 (solid), D1S (dashed), SP (dotted), IPM (dashed-dotted), and global (dashed-dotted-dotted) densities of  ${}^{208}\text{Pb}$ . The inset figure illustrates these nuclear densities.

For the density of the  ${}^{208}\text{Pb}$  daughter nucleus, we consider five different parametrizations. First, microscopic Hartree-Fock-Bogoliubov (HFB) calculations are performed with zero-range BSk14 Skyrme<sup>33</sup> and finite-range D1S Gogny<sup>34,35</sup> interactions to give the densities, which we also denoted BSk14 and D1S, respectively. The HFB calculations using both effective NN interactions have been extensively tested for the mass region near  ${}^{208}\text{Pb}$  and proved to be highly reliable when describing the bulk properties (such as densities) in that region. It is noted that the matter densities from these microscopic calculations are also included in the IAEA Reference Input Parameter Library (RIPL-3)<sup>36</sup>. We also consider a much simpler mean-field model, known as the independent particle model (IPM), where the single-particle states are generated from the Woods-Saxon potentials with parameters taken from the classic work of Bohr and Motelson<sup>37</sup>. Next, we consider two density parametrizations using the 2-parameter Fermi (2pF) distribution. The first parametrization by the Sao Paulo group<sup>38</sup>, which we call SP, is obtained from a systematic fitting to the Dirac-Hartree-Bogoliubov results<sup>39</sup>. This parametrization, which is often incorporated with the Sao Paulo folding model<sup>38</sup>, is widely used in many heavy-ion scattering studies. Finally, a fixed parameter set of  $R=1.07A^{1/3}$  fm and  $a=0.54$  fm for the 2pF is used for the “Global” density<sup>40</sup>. This fixed shape for 2pF density is often used in some DFM calculations of  $\alpha$ -decay half-lives<sup>13,14,31</sup>. The five mentioned

densities BSk14, D1S, SP, IPM, and Global along with their corresponding DFM calculations are presented in Figure 1.

### The folding potential description of nuclear rainbow $\alpha + {}^{208}\text{Pb}$ scattering

To clearly observe the impact of the  ${}^{208}\text{Pb}$  density on the double-folding potential, we use the potentials illustrated in Figure 1 to reproduce the differential cross section for the elastic scattering of  $\alpha$  particles by the  ${}^{208}\text{Pb}$  nucleus. To calculate the cross section, we perform an optical model analysis for the elastic  $\alpha + {}^{208}\text{Pb}$  scattering data in which the optical potential is composed of the renormalized double-folding and Coulomb potentials described in the previous section and a standard Woods-Saxon imaginary potential, i.e.,. The renormalization factor and the Woods-Saxon parameters are listed in Table 1. The incident energy of the  $\alpha$  projectile is chosen at 139 MeV, where the high resolution data are measured by Goldberg *et al.* at the University of Maryland<sup>19</sup>. Although there are many elastic  $\alpha + {}^{208}\text{Pb}$  scattering data at different energies (see Ref.<sup>41</sup> and references therein), only the data at 139 MeV<sup>19</sup> display a clear refractive rainbow pattern.

Figure 2 presents the experimental differential cross section data<sup>19</sup> and the optical model results using the double-folding potentials calculated with the BSk14, D1S, SP, IPM, and global densities of  ${}^{208}\text{Pb}$ .

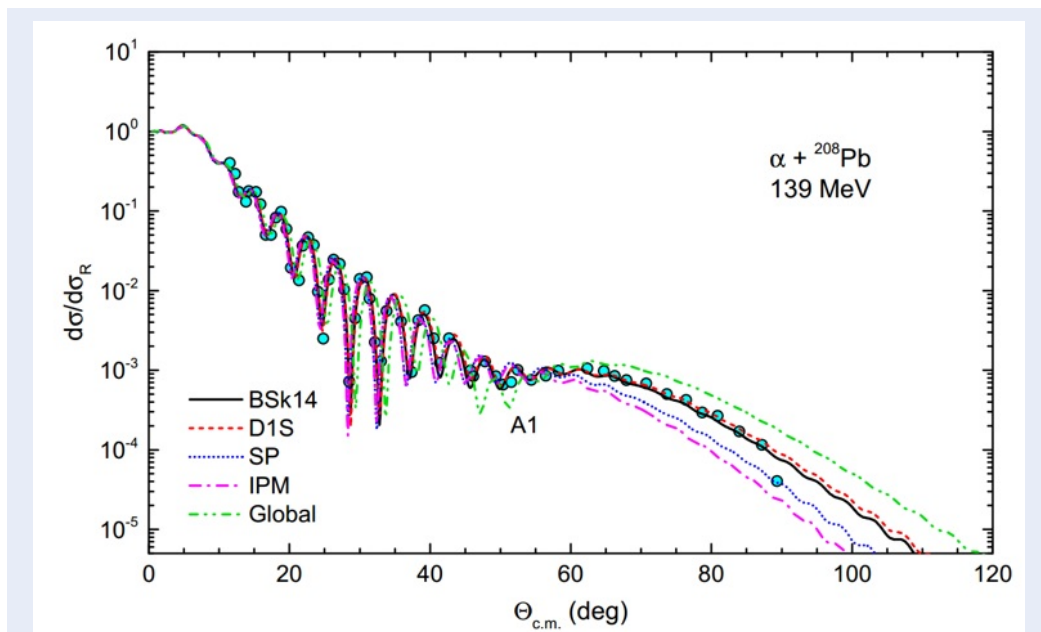


**Figure 2:** Differential cross section of elastic  $\alpha + {}^{208}\text{Pb}$  scattering at 139 MeV. The experimental data <sup>19</sup> are compared with the optical model results using the folding potentials calculated from the BSk14 (solid), D1S (dashed), SP (dotted), IPM (dashed-dotted), and global (dashed-dotted-dotted) densities of  ${}^{208}\text{Pb}$ . The position of the first Airy minimum is labeled A1.

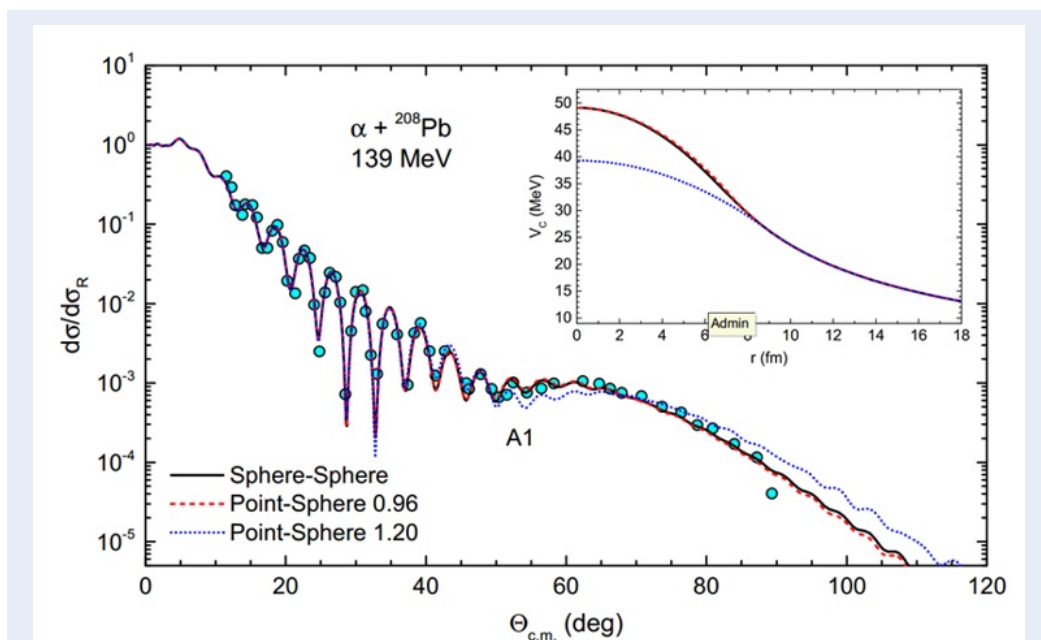


**Figure 3:** Differential cross section of elastic  $\alpha + {}^{208}\text{Pb}$  scattering at 139 MeV. The experimental data <sup>19</sup> are compared with the optical model results using the folding potentials calculated from the BSk14 density and the sphere-sphere (solid), point-sphere with  $r_C = 0.96$  fm (dashed), and point-sphere with  $r_C = 1.2$  fm (dotted) descriptions of the Coulomb potentials.

**Table 1: The best-fit parameters of the optical potential for the elastic  $\alpha + {}^{208}\text{Pb}$  scattering at 139 MeV.  $N_R$  is the renormalization factor of the real folding potential**

	$N_R$	$W_0$ (MeV)	$R$ (fm)	$a$ (fm)
BSk14	0.920	21.13	8.706	0.723
D1S	0.932	21.57	8.652	0.725
SP	0.905	22.46	8.745	0.725
IPM	0.912	22.81	8.762	0.701
Global	0.915	18.69	8.647	0.705

In addition to the nuclear potential, another important ingredient in the  $\alpha$ -decay calculation is the Coulomb potential. In our calculation, we calculate the Coulomb potential by folding two uniform charge spheres<sup>26</sup> with radii constrained by experimental RMS charge radii, a procedure we referred to as the sphere-sphere description. Many  $\alpha$ -decay studies, such as Refs.<sup>4,10-13</sup> use a simpler and more common procedure that treats the projectile as a point charge interacting with a uniform charge sphere of the target with the Coulomb radius defined as  $R_C = r_C (A_p^{1/3} + A_t^{1/3})$ . The effect of the  $r_C$  parameter in the point-sphere Coulomb formalism on the elastic scattering cross section is investigated and illustrated in Figure 3.

### Impacts of nuclear density on the $\alpha$ -decay half-life of ${}^{212}\text{Po}$

In this final part, we apply the folding potentials generated above to the semiclassical preformed cluster model to calculate the  $\alpha$ -decay half-life of  ${}^{212}\text{Po}$ . The experimental Q-value of this decay is 8.954 MeV<sup>42</sup>. The theoretical half-life  $T_{1/2}^{cal}$  is calculated assuming a complete cluster model with  $P_\alpha = 1$  and thus cannot be compared directly with the experimental value without applying a realistic  $\alpha$  preformation factor. Since this  $\alpha$  preformation factor is not well determined, we use the standard formula  $P_\alpha^{exp} = T_{1/2}^{cal} / T_{1/2}^{exp}$  to extract the “experimental”  $\alpha$  preformation factor<sup>43</sup> and then compare it with some microscopic and empirical values in the literature. The  $\alpha$ -decay half-lives calculated with the DFM using various choices of densities and the experimental value<sup>44</sup> are presented in Table 2.

## DISCUSSION

In contrast to the surface region, all considered densities are rather different in the interior region. Due to the simple 2pF shape, the SP and global densities have smooth shapes in the interior region, while those using single-particle calculations (BSk14, D1S, IPM)

display oscillation structures due to the contribution of the squared single-particle radial wave functions. It is known that the refractive rainbow scattering can probe even into this interior region<sup>8,17</sup>.

We now consider the capability of the five folding potentials illustrated in Figure 1 to describe the nuclear rainbow scattering. As shown in Figure 2, a very clear first Airy minimum can be seen at a scattering angle  $\approx 50^\circ$  in the experimental data. From now on, we refer to a specific potential by the name of the density parametrization used in its folding procedure. The small (forward) scattering angular region before the A1 minimum with rapid oscillations is known as the Fraunhofer diffraction region<sup>8,17</sup>, where the surface part of the potential contributes dominantly. Figure 2 shows that all potentials can reproduce this region with good quality, except for the global potential, which shows a slightly out-of-phase behavior.

For the rainbow region around and after the A1 minimum, the differences between the five considered potentials are greatly enhanced as the reaction can now probe deeper into the interior region of the nucleus. Two potentials obtained from the sophisticated HFB calculations with BSk14 and D1S give the best agreement with the measured data for the angular region up to  $90^\circ$ . The IPM, SP, and global potentials fail to describe the fallout after A1 in the cross section. We note that since Figure 2 is plotted on the logarithmic scale, the deviation of the global potential result from the experimental data is much larger than those from the IPM and SP potentials. The amount of agreement between the cross sections calculated with the five density parametrizations and the experimental data is as expected since the BSk14 and D1S HFB calculations are specifically performed for the  ${}^{208}\text{Pb}$  nucleus using two of the best phenomenological interactions. On the other extreme, the global density uses a fixed set of a few parameters to describe the 2pF distribution for all nuclei, which explains its discrepancy with the data. From the results in Figure 2, we can conclude that the density used in the DFM calculation can be

**Table 2: The theoretically calculated  $\alpha$ -decay half-lives of  $^{212}\text{Po}$  and the experimentally extracted  $\alpha$  preformation factor**

Density	BSk14	D1S	SP	IPM	Global	Exp. <sup>44</sup>
$T_{1/2}$ (s)	6.386E-09	6.950E-09	3.933E-09	4.135E-09	1.421E-08	2.944E-07
$P_{\alpha}^{exp}$	0.0217	0.0236	0.0133	0.0140	0.0483	

unambiguously constrained using the nuclear rainbow scattering cross section.

In addition, we illustrate in **Figure 3** that the point-sphere Coulomb interaction with a suitably chosen  $r_C$  parameter can approximate the more sophisticated sphere-sphere Coulomb description with good accuracy. In particular, the value of  $r_C = 0.96$  fm provides a very similar result to the Coulomb potential using the sphere-sphere description. As a result, the point-sphere Coulomb potential with  $r_C = 0.96$  fm provides a better description of the measured elastic  $\alpha + ^{208}\text{Pb}$  scattering cross section than that using  $r_C = 1.2$  fm. This shows that the effect of the  $r_C$  parameter can also be observed on the rainbow scattering cross section. In the present work, we only use the point-sphere and sphere-sphere approximations to describe the Coulomb potential. For a more realistic description, a double-folding procedure could be required to calculate the Coulomb interaction.

Finally, we consider the impacts of nuclear density on the  $\alpha$ -decay half-life of  $^{212}\text{Po}$ . By looking at the pure half-life values in **Table 2**, one can see a strong correspondence between these values and the choices of  $^{208}\text{Pb}$  daughter nuclear densities. The largest half-life value of the global potential is larger than the smallest value of the SP potential by a factor of 3.6. The extracted  $\alpha$  preformation factors of the two most realistic choices of density, BSk14 and D1S, are 0.0217 and 0.0236, respectively. These values are in very good agreement with the calculated  $\alpha$  preformation factor or the  $\alpha$  spectroscopic factor values in other studies, such as 0.035<sup>43</sup>, 0.027<sup>43</sup>, and 0.025<sup>22</sup>. These results show that a folding potential capable of describing the rainbow scattering cross section will give a realistic value for the  $\alpha$ -decay half-life. They also justify the use of the HFB model with the BSk14 and D1S interactions to calculate the density of the daughter nucleus in the  $\alpha$ -decay calculation.

## CONCLUSION

We have performed the DFM calculation to generate the nuclear potentials using several choices of  $^{208}\text{Pb}$  densities. These potentials are then used to calculate the cross section of the elastic  $\alpha + ^{208}\text{Pb}$  scattering at 139 MeV, which exhibits a clear nuclear rain-

bow pattern. We found that the theoretical cross sections corresponding to the HFB calculations with the BSk14 and D1S densities are in the best agreement with the experimental data, especially around the refractive Airy minimum. We also illustrate the impact of the Coulomb radius on the calculated rainbow scattering cross section and justify the use of a simple point-sphere formula for the Coulomb potential. Finally, we note the strong correlation between the folding potential ability to describe the nuclear rainbow pattern and the calculated  $\alpha$ -decay half-life. The extracted  $\alpha$  preformation factors using the realistic choices of the BSk14 and D1S densities give excellent agreement with other results in the literature. Our results suggest that the nuclear rainbow scattering phenomenon is a useful tool to constrain the nuclear potential and provide a reliable  $\alpha$ -decay half-life within the preformed cluster model.

## LIST OF ABBREVIATIONS

DFM: Double-folding model  
 HFB: Hartree-Fock-Bogoliubov  
 IPM: Independent particle model  
 NN: Nucleon-nucleon  
 RIPL-3: Reference input parameter library  
 RMS: Root-mean-square  
 SP: Sao Paulo  
 WKB: Wentzel-Kramers-Brillouin

## COMPETING INTERESTS

The authors declare that they have no conflicts of interest.

## ACKNOWLEDGMENTS

We thank Prof. Dao T. Khoa for useful discussion related to the double-folding model. The present research was supported, in part, by Vietnam National University, Ho Chi Minh City, Vietnam under grant C2019-18-02.

## AUTHORS' CONTRIBUTIONS

All authors significantly contributed to this work and approved the article for publication.

## REFERENCES

1. Lovas RG, Liotta RJ, Insolia A, Varga K, Delion DS. Microscopic theory of cluster radioactivity, *Physics Reports*. 1998; 294: 265-362; Available from: [https://doi.org/10.1016/S0370-1573\(97\)00049-5](https://doi.org/10.1016/S0370-1573(97)00049-5).
2. Pfützner M, Karny M, Grigorenko LV, Riisager K. Radioactive decays at limits of nuclear stability, *Reviews of Modern Physics*. 2012; 84: 567-619; Available from: <https://doi.org/10.1103/RevModPhys.84.567>.
3. Qi C, Liotta R, Wyss R. Recent developments in radioactive charged-particle emissions and related phenomena, *Progress in Particle and Nuclear Physics*. 2019; 105: 214-251; Available from: <https://doi.org/10.1016/j.pnpnp.2018.11.003>.
4. Buck B, Merchant AC, Perez SM. Half-Lives of Favored Alpha Decays from Nuclear Ground States, *Atomic Data and Nuclear Data Tables*. 1993; 54: 53-73; Available from: <https://doi.org/10.1006/adnd.1993.1009>.
5. Belli P, Bernabei R, Danevich FA, Incicchitti A, Tretyak VI. Experimental searches for rare alpha and beta decays, *European Physical Journal A*. 2019; 55: 140; Available from: <https://doi.org/10.1140/epja/i2019-12823-2>.
6. Hofmann S, Münzenberg G. The discovery of the heaviest elements, *Reviews of Modern Physics*. 2000; 72: 733-767; Available from: <https://doi.org/10.1103/RevModPhys.72.733>.
7. Oganessian YT, Utyonkov VK. Superheavy element research, *Reports on Progress in Physics*. 2015; 78: 036301; Available from: <https://doi.org/10.1088/0034-4885/78/3/036301>.
8. Brandan ME, Satchler GR. The interaction between light heavy-ions and what it tells us, *Physics Reports*. 1997; 285: 143-243; Available from: [https://doi.org/10.1016/S0370-1573\(96\)00048-8](https://doi.org/10.1016/S0370-1573(96)00048-8).
9. Khoa DT.  $\alpha$ -nucleus optical potential in the double-folding model, *Physical Review C*. 2001; 63: 034007; Available from: <https://doi.org/10.1103/PhysRevC.63.034007>.
10. Buck B, Merchant AC. Cluster-model calculations of exotic decays from heavy nuclei, *Physical Review C*. 1989; 39: 2097-2100(R); Available from: <https://doi.org/10.1103/PhysRevC.39.2097>.
11. Mohr P.  $\alpha$ -nucleus potentials for the neutron-deficient p nuclei, *Physical Review C*. 2000; 61: 045802. Available from: <https://doi.org/10.1103/PhysRevC.61.045802>; Available from: <https://doi.org/10.1103/PhysRevC.61.045802>.
12. Basu DN. Folding model analysis of alpha radioactivity, *Journal of Physics G*. 2003; 29: 2079-2085. Available from: <http://dx.doi.org/10.1088/0954-3899/29/9/303>; Available from: <https://doi.org/10.1088/0954-3899/29/9/303>.
13. Xu C, Ren Z. Systematical calculation of  $\alpha$  decay half-lives by density-dependent cluster model, *Nuclear Physics A*. 2005; 753: 174-185; Available from: <https://doi.org/10.1016/j.nuclphysa.2005.02.125>.
14. Ismail M, Ellithi AY, Botros MM, Adel A. Systematics of  $\alpha$ -decay half-lives around shell closures, *Physical Review C*. 2010; 81: 024602; Available from: <https://doi.org/10.1103/PhysRevC.81.024602>.
15. Satchler GR, Love WG. Folding model potentials from realistic interactions for heavy-ion scattering, *Physics Reports*. 1979; 55: 183-254; Available from: [https://doi.org/10.1016/0370-1573\(79\)90081-4](https://doi.org/10.1016/0370-1573(79)90081-4).
16. Mohr P.  $\alpha$ -nucleus potentials,  $\alpha$ -decay half-lives, and shell closures for superheavy nuclei, *Physical Review C*. 2006; 73: 031301(R); Available from: <https://doi.org/10.1103/PhysRevC.73.031301>.
17. Khoa DT, von Oertzen W, Bohlen HG, Ohkubo S. Nuclear rainbow scattering and nucleus-nucleus potential, *Journal of Physics G*. 2007; 34: R111-R164; Available from: <https://doi.org/10.1088/0954-3899/34/3/R01>.
18. Goldberg DA, Smith SM. Criteria for the elimination of discrete ambiguities in nuclear optical potentials, *Physical Review Letters*. 1972; 29: 500-503; Available from: <https://doi.org/10.1103/PhysRevLett.29.500>.
19. Goldberg DA, Smith SM, Pugh HG, Roos PG, Wall NS. Scattering of 139-MeV Alpha Particles by 58Ni and 208Pb, *Physical Review C*. 1973; 7: 1938-1950; Available from: <https://doi.org/10.1103/PhysRevC.7.1938>.
20. Goldberg DA, Smith SM, Burdzik GF. Refractive behavior in intermediate-energy alpha scattering, *Physical Review C*. 1974; 10: 1362-1371; Available from: <https://doi.org/10.1103/PhysRevC.10.1362>.
21. Michel F, Ohkubo S, Reidemeister G. Local Potential Approach to the Alpha-Nucleus Interaction and Alpha-Cluster Structure in Nuclei, *Progress of Theoretical Physics Supplement*. 1998; 132: 7-72; Available from: <https://doi.org/10.1143/PTP.132.7>.
22. Varga K, Lovas RG, Liotta RJ. Absolute alpha decay width of 212Po in a combined shell and cluster model, *Physical Review Letters*. 1992; 69: 37-40; Available from: <https://doi.org/10.1103/PhysRevLett.69.37>.
23. Buck B, Merchant AC, Perez SM. Alpha-cluster structure in 212Po, *Physical Review Letters*. 1994; 72: 1326-1328; Available from: <https://doi.org/10.1103/PhysRevLett.72.1326>.
24. Xu C, Ren Z, Ropke G, Schuck P, Funaki Y, Horiuchi H, Tohsaki A, Yamada T, Zhou B.  $\alpha$ -decay width of 212Po from a quark-tetting wave function approach, *Physical Review C*. 2016; 93: 011306(R); Available from: <https://doi.org/10.1103/PhysRevC.93.011306>.
25. Campi X, Bouyssy A. A simple approximation for the nuclear density matrix, *Physics Letters B*. 1978; 73: 263-266; Available from: [https://doi.org/10.1016/0370-2693\(78\)90509-9](https://doi.org/10.1016/0370-2693(78)90509-9).
26. Poling JE, Norbeck E, Carlson RR. Elastic scattering of lithium by 9Be, 10B, 12C, 13C, 16O, and 28Si from 4 to 63 MeV, *Physical Review C*. 1976; 13: 648-660; Available from: <https://doi.org/10.1103/PhysRevC.13.648>.
27. De Vries H, De Jager CW, De Vries C. Nuclear charge-density-distribution parameters from elastic electron scattering, *Atomic Data and Nuclear Data Tables*. 1987; 36: 495-536; Available from: [https://doi.org/10.1016/0092-640X\(87\)90013-1](https://doi.org/10.1016/0092-640X(87)90013-1).
28. Hahn B, Ravenhall DG, Hofstadter R. High-energy electron scattering and the charge distributions of selected nuclei, *Physical Review*. 1956; 101: 1131-1142; Available from: <https://doi.org/10.1103/PhysRev.101.1131>.
29. Khoa DT, Satchler GR, von Oertzen W. Nuclear incompressibility and density dependent NN interactions in the folding model for nucleus-nucleus potentials, *Physical Review C*. 1997; 56: 954-969; Available from: <https://doi.org/10.1103/PhysRevC.56.954>.
30. Anantaraman N, Toki H, Bertsch GF. An effective interaction for inelastic scattering derived from the Paris potential, *Nuclear Physics A*. 1983; 398: 269-278; Available from: [https://doi.org/10.1016/0375-9474\(83\)90487-6](https://doi.org/10.1016/0375-9474(83)90487-6).
31. Ismail M, Adel A. Effect of deformation parameters, Q value, and finite-range NN force on  $\alpha$ -particle preformation probability, *Physical Review C*. 2014; 89: 034617; Available from: <https://doi.org/10.1103/PhysRevC.89.034617>.
32. Wildermuth K, Tang YC. *A Unified Theory of the Nucleus*, Academic Press, New York. 1977; Available from: <https://doi.org/10.1007/978-3-322-85255-7>.
33. Goriely S, Samyn M, Pearson JM. Further explorations of Skyrme-Hartree-Fock-Bogoliubov mass formulas. VII. Simultaneous fits to masses and fission barriers, *Physical Review C*. 2007; 75: 064312; Available from: <https://doi.org/10.1103/PhysRevC.75.064312>.
34. Dechargé J, Gogny D. Hartree-Fock-Bogolyubov calculations with the D1 effective interaction on spherical nuclei, *Physical Review C*. 1980; 21: 1568-1593; Available from: <https://doi.org/10.1103/PhysRevC.21.1568>.
35. Hilaire S, Girod M. Large-scale mean-field calculations from proton to neutron drip lines using the D15 Gogny force, *European Physical Journal A*. 2007; 33: 237-241; Available from: <https://doi.org/10.1140/epja/i2007-10450-2>.
36. Reference Input Parameter Library (RIPL-3) <https://www.nds.iaea.org/RIPL-3/> Available online on November 6th, 2021;

37. Bohr A, Mottelson BR. Nuclear structure volume 1: Single-particle motion, World Scientific, Singapore. 1969;
38. Chamon LC, Carlson BV, Gasques LR, Pereira D, De Conti C, Alvarez MAG, Hussein MS, Cândido Ribeiro MA, Rossi Jr ES, Silva CP. Toward a global description of the nucleus-nucleus interaction, *Physical Review C*. 2002; 66: 014610; Available from: <https://doi.org/10.1103/PhysRevC.66.014610>.
39. Carlson BV, Hirata D. Dirac-Hartree-Bogoliubov approximation for finite nuclei, *Physical Review C*. 2000; 62: 054310; Available from: <https://doi.org/10.1103/PhysRevC.62.054310>.
40. Walecka JD. *Theoretical Nuclear Physics and Subnuclear Physics*, Oxford Univ. Press, Oxford. 1995;
41. Pang DY, Ye YL, Xu FR. Application of the Bruyeres Jeukenne-Lejeune-Mahaux model potential to composite nuclei with a single-folding approach, *Physical Review C*. 2011; 83: 064619; Available from: <https://doi.org/10.1103/PhysRevC.83.064619>.
42. Wang M, Huang W, Kondev F, Audi G, Naimi S. The AME 2020 atomic mass evaluation (II). Tables, graphs and references, *Chinese Physics C*. 2021; 45: 030003; Available from: <https://doi.org/10.1088/1674-1137/abddb0>.
43. Seif WM. The  $\alpha$  decay spectroscopic factor of heavy and superheavy nuclei, *Journal of Physics G*. 2013; 40: 105102; Available from: <https://doi.org/10.1088/0954-3899/40/10/105102>.
44. Kondev F, Wang M, Huang W, Naimi S, Audi G. The NUBASE2020 evaluation of nuclear physics properties, *Chinese Physics C*. 2021; 45: 030001; Available from: <https://doi.org/10.1088/1674-1137/abddae>.

# Tạp chí Phát triển Khoa học và Công nghệ Đại học Quốc gia Tp. Hồ Chí Minh



**Tạp chí Phát triển Khoa học và Công nghệ**

**ISSN: 1859-0128**

**Hình thức xuất bản:** In và trực tuyến

**Hình thức truy cập:** Truy cập mở (Open Access)

**Ngôn ngữ bài báo:** Tiếng Anh

**Tỉ lệ chấp nhận đăng 2021:** 72%

**Phí xuất bản:** Miễn phí

**Thời gian phản biện:** 43 ngày

**Lập chỉ mục (Indexed):** Google Scholar, Scilit



SCAN ME



**Tạp chí Phát triển Khoa học và Công nghệ -  
Khoa học Tự nhiên**

**ISSN: 2588-106X**

**Hình thức xuất bản:** In & trực tuyến

**Hình thức truy cập:** Truy cập mở

**Ngôn ngữ bài báo:** Tiếng Việt

**Tỉ lệ chấp nhận đăng 2021:** 75%

**Phí xuất bản:** Miễn phí

**Thời gian phản biện:** 30-45 ngày

**Lập chỉ mục (Indexed):** Google Scholar, Scilit



SCAN ME



**Tạp chí Phát triển Khoa học và Công nghệ -  
Kỹ thuật và Công nghệ**

**ISSN: 2615-9872**

**Hình thức xuất bản:** In & trực tuyến

**Hình thức truy cập:** Truy cập mở

**Ngôn ngữ bài báo:** Tiếng Việt

**Tỉ lệ chấp nhận đăng 2021:** 61%

**Phí xuất bản:** Miễn phí

**Thời gian phản biện:** 50 ngày

**Lập chỉ mục (Indexed):** Google Scholar, Scilit



SCAN ME



**Tạp chí Phát triển Khoa học và Công nghệ -  
Kinh tế-Luật và Quản lý**

**ISSN: 2588-1051**

**Hình thức xuất bản:** In & trực tuyến

**Hình thức truy cập:** Truy cập mở

**Ngôn ngữ bài báo:** Tiếng Việt

**Tỉ lệ chấp nhận đăng 2021:** 65%

**Phí xuất bản:** Miễn phí

**Thời gian phản biện:** 45 ngày

**Lập chỉ mục (Indexed):** Google Scholar, Scilit



SCAN ME



**Tạp chí Phát triển Khoa học và Công nghệ -  
Khoa học Xã hội và Nhân văn**

**ISSN: 2588-1043**

**Hình thức xuất bản:** In & trực tuyến

**Hình thức truy cập:** Truy cập mở

**Ngôn ngữ bài báo:** Tiếng Việt

**Tỉ lệ chấp nhận đăng 2021:** 62%

**Phí xuất bản:** Miễn thu phí đối với tác giả là CBVC của ĐHKHXHNV, ĐHQG-HCM; Tác giả khác: 500.000 VNĐ/bài

**Thời gian phản biện:** 75 ngày

**Lập chỉ mục (Indexed):** Google Scholar, Scilit



SCAN ME



**Tạp chí Phát triển Khoa học và Công nghệ -  
Khoa học Trái đất và Môi trường**

**ISSN: 2588-1078**

**Hình thức xuất bản:** In & trực tuyến

**Hình thức truy cập:** Truy cập mở

**Ngôn ngữ bài báo:** Tiếng Việt và tiếng Anh

**Tỉ lệ chấp nhận đăng 2021:** 87%

**Phí xuất bản:** liên hệ tòa soạn

**Thời gian phản biện:** 45 ngày

**Lập chỉ mục (Indexed):** Google Scholar, Scilit



SCAN ME



**Tạp chí Phát triển Khoa học và Công nghệ -  
Khoa học Sức khỏe**

**ISSN: 2734-9446**

**Hình thức xuất bản:** In & trực tuyến

**Hình thức truy cập:** Truy cập mở

**Ngôn ngữ bài báo:** Tiếng Việt

**Tỉ lệ chấp nhận đăng 2021:** 70%

**Phí xuất bản:** Miễn phí

**Thời gian phản biện:** 30 ngày

**Lập chỉ mục (Indexed):** Google Scholar, Scilit



SCAN ME

*Tạp chí Phát triển Khoa học và Công nghệ, Đại học Quốc gia Tp.HCM*

*25 năm xuất bản học thuật (1997-2022)*

Tòa soạn: Nhà điều hành Đại học Quốc gia Tp.HCM, P. Linh Trung, TP. Thủ Đức, TP. HCM

Email: [stj@vnuhcm.edu.vn](mailto:stj@vnuhcm.edu.vn); [tcptkcn@vnuhcm.edu.vn](mailto:tcptkcn@vnuhcm.edu.vn); Website: <http://www.scienceandtechnology.com.vn>